3.1. Introduction

The biologically active benzimidazole and its derivatives have also a significant importance to various industrial applications, including the production of drugs, pigments, and chemical UVB filters.[1],[2],[3] Benzimidazoles play a crucial role as the foundational components in natural products, pharmaceuticals, and organic/polymeric materials.[4],[5],[6] The use of benzimidazoles for antibacterial, antifungal, antiinflammatory, antiulcer, anticancer, and anti-HIV activities is well established.[7],[8],[9],[10],[11] Traditionally, benzimidazoles are synthesized by the condensation of 1,2-diaminobenzene with carboxylic acids or their derivatives (such as acyl chlorides, acids, anhydrides, amides, and nitriles) under highly acidic conditions at elevated temperatures.[5],[4],[12]

In the past few decades, transition metal-based (Pd,[13],[14],[15] Pt,[16] Ru,[3],[17],[18] Ir,[19],[20] etc.)[21],[22] homogeneous catalysts have been used for benzimidazole synthesis.[23],[24],[25] These catalysts provide excellent activity and selectivity for the reaction.[22],[26],[27] However, homogeneous catalysts have many disadvantages such as high-cost, poor recyclability, and use of expensive additive ligands.[28],[29],[30] In recent years, 3d transition metal (Ni,[31],[32] Co,[33],[34] Cu,[35] Zn,[36],[37] Fe,[38] etc.)[29]-based heterogeneous catalysts have been demonstrated for the benzimidazole synthesis.[39],[40] These catalysts offer high catalytic activity and selectivity towards benzimidazole formation.[41],[42]

In recent years, metal nitrogen-doped carbon (M−N−C@NC) nanocatalysts have been explored in different fields such as electrochemistry and organic transformation reactions.[43],[44],[45] The M−N−C@NC nanocatalysts provided excellent catalytic activity for the organic reactions. In chapter 1 and chapter 2, we have already discussed the importance of the MOF-derived M−N−C@NC catalyst for the organic transformation reactions.[46,47,48,49,50,51]

In this chapter, we have explored the Co−N−C@NC catalyst for the benzimidazole formation by the reaction of *o*-phenylenediamine with alcohols (**Scheme 3.1**). The Co−N−C@NC catalyst provided excellent catalytic activity for the benzimidazole formation. The N−doped carbon and N−doped CNTs support enhanced the catalytic stability and electron transfer in Co−N−C@NC catalyst and also improved the yield (>90%) of benzimidazole formation. The Co−N−C@NC works as a hydrogen transfer via coupling for the benzimidazole reactions. Furthermore, the catalyst demonstrated enough stability for five consecutive catalytic cycles, maintaining its catalytic activity and selectivity.

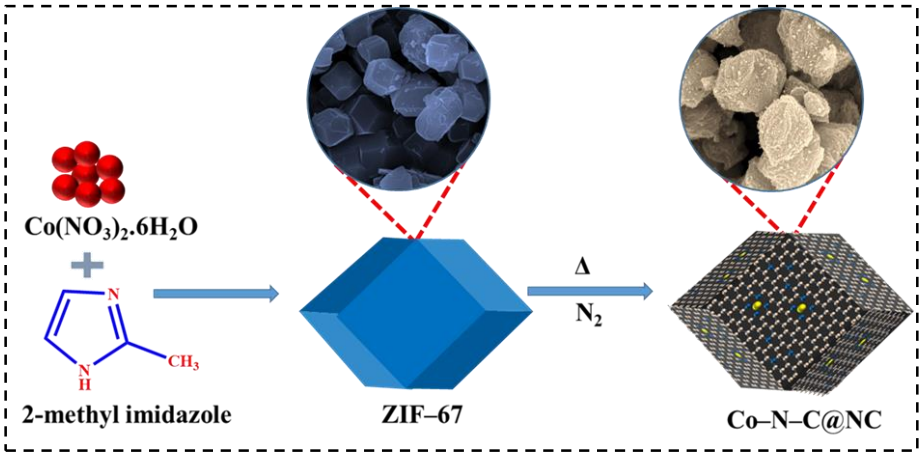

Scheme 3.1: Schematic representation for the synthesis of Co−N−C@NC catalyst.

3.2. Chemicals

o-phenylenediamine derivatives were purchased from various chemical companies (Sigma Aldrich, Avra, Alfa Aesar, and SRL Pvt. Ltd. India), and the rest of the chemicals were mentioned in chapter 2, section 2.2.

3.3. Instruments

The same instruments were used for the spectroscopic, microscopic and NMR characterization of the catalysts and products as mentioned in chapter 2, section 2.3.

3.4. Experimental

3.4.1. Synthesis of ZIF-67[52]

$Co(NO_3)_2.6H_2O$ (1 mmol) was dissolved in 20 mL methanol solution and stirred 10 minutes to form dispersion A. 2-methylimidazole (4 mmol) was separately dissolved in 20 mL methanol and stirred for 10 minutes to form dispersion B. Then, dispersion B was added to A at a time and stirred for 30 minutes and then stayed for 24 h. The precipitate was collected by centrifugation (14000) and washed three times with methanol and dried overnight at 60 ºC. And it was denoted as ZIF-67.

3.4.2. Synthesis of Co−N−C@NC[53]

300 mg of ZIF-67 was ground in a mortar pestle to get a fine powder. The powder was placed in a crucible boat and heated at 800 °C in the presence of N_2 for 3 h (in a tubular furnace with a heating rate: 5 °C/min from 35 °C). The furnace was allowed to cool down to room temperature. The black powder was collected and denoted as Co−N−C@NC. Similarly, the synthesis of Co−N−C@NC−1 and Co−N−C@NC−

3.4.3. Synthesis of Co@C

The synthesis of Co@C is mentioned in chapter 2 section 2.3.3.

3.5. Results and discussion

3.5.1. Characterizations of the catalysts

The precursor ZIF-67 was prepared through the reaction of cobalt(II) nitrate and 2-methylimidazole (**Scheme 3.1**). The Powder X-ray diffraction (PXRD) analysis revealed the characteristic crystal planes of ZIF-67 (**JCPDS: 08-60-513, shown in Figure 3.1a**).[52] The SEM images showed the dodecahedron morphology of ZIF-67 (**Figure 3.1b**).[54] The EDX of ZIF-67 confirmed the presence of Co, N, and C. The elemental mapping of the ZIF-67

confirmed that the elements were homogeneously distributed (**Figure 3.1c-g**).

The precursor material ZIF-67 was pyrolyzed in an inert atmosphere at various temperatures (at 700, 800, and 900 ºC) to produce Co−N−C@NC. The PXRD pattern of Co−N−C@NC nanoparticles revealed the face-centered cubic (fcc) crystal structure of cobalt (**JCPDS: No.15-0806, Figure 3.1c**).[52] The graphitic carbon peaks were observed at 2 theta value 25.8º showing the corresponding plane (002). In Co−N−C@NC, the (111) peak of cubic cobalt showed a slight rightward shift (2θ = 0.2º) due to nitrogen coordination (JCPDS: 08-60-513).

Further, Raman spectroscopy was carried out to realize the degree of graphitization of N-doped carbon (NC) in Co−N−C@NC. The Raman spectrum showed two characteristic bands for D and G at 1326.0 and 1588.6 cm^{-1}, respectively (**Figure. 3.1d**). The I_D/I_G ratio of 1.44 indicates a defect-rich structure of graphene. The classical A_{1g} vibronic modes of metallic Co were detected at 674.4 cm^{-1}.[55]

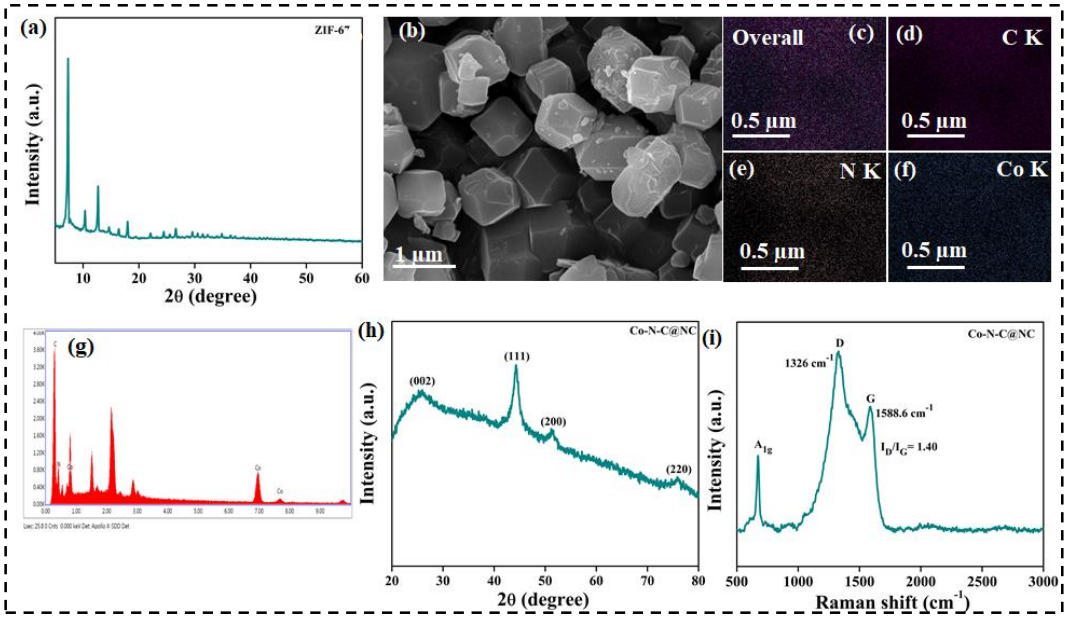

Figure 3.1: (a) The PXRD pattern of ZIF-67. (b) The SEM image shows the dodecahedron morphology of ZIF-67 and (c-f) images shows the elemental mapping, (g) EDX spectra of ZIF-67. (h) PXRD of Co−N−C@NC, (i) Raman spectrum of Co−N−C@NC catalyst.

The nature of carbon further confirmed by the XPS spectra of the Co−N−C@NC (**Figure 3.2**). The C 1s XPS spectrum was deconvoluted into four peaks for C=C and C=N with the corresponding binding energy 284.2 eV and 285.6 eV of the sp^2 hybridized carbon and sp^3 hybridized carbon peaks of C−C (284.7 eV) and C−N (287.7 eV). The ratio of graphitic carbon to the other carbon is 1.39 and it is close to the peak ratio obtained from the Raman spectrum of Co−N−C@NC (**Figure 3.2a**).[56]

The N 1s XPS spectrum was fitted into four peaks for pyridinic, Co−N, pyrrolic, and graphitic nitrogen with binding energies 398.4, 399.0, 399.9, and 400.8 eV, respectively. This result shows that the Co−N bond was present in Co−N−C@NC. The Co was strongly bonded with the different N-moieties (pyridinic−N, pyrollic−N, and graphitic−N, **Figure 3.2b**).[57],[58]

The Co 2p XPS was deconvoluted into two peaks Co $2p_{3/2}$ and Co $2p_{1/2}$ with corresponding binding energy 779.4 and 795.0 eV. Further, Co $2p_{3/2}$ XPS peak was deconvoluted into three peaks with corresponding Co(0) (779.1 eV), Co(II) (780.1 eV), and Co-N (781.5 eV). The Co $2p_{1/2}$ peak was fitted into two peaks for Co^0 (794.1 eV) and Co^{2+} (795.8 eV) respectively. The satellite peaks of the Co 2p XPS was observed at 784.5, 788.2 and 803.0 eV (**Figure 3.2c**).[59]

The SEM image showed the dodecahedron morphology of the Co−N−C@NC (**Figure 3.2d**). The EDX spectrum Co−N−C@NC confirmed Co, N, and C elements, and the elemental mapping confirmed that the elements Co, N, and C were homogeneously distributed.

Furthermore, the morphological details were confirmed by TEM (**Figure 3.2e**). The TEM image confirmed that the Co nanoparticles supported on carbon nanotubes (CNTs) and N-doped carbon (NC) (**Figure 3.2f-g**). The SAED pattern of Co−N−C@NC revealed diffraction rings for the crystal planes (111), (200), and (220) of *fcc* cobalt (**Figure 3.2g-inset)**. The HR-TEM detected d-spacing of 0.207 nm- corresponding to plane (111) of *fcc* cobalt center and

0.36 nm- corresponding to (002) plane of graphene (**Figure 3.2h)**. The TEM images of Co−N−C@NC illustrated the distribution of cobalt nanoparticles of various sizes (2-10 nm) within the nitrogen-doped carbon frameworks (**Figure 3.2i**).

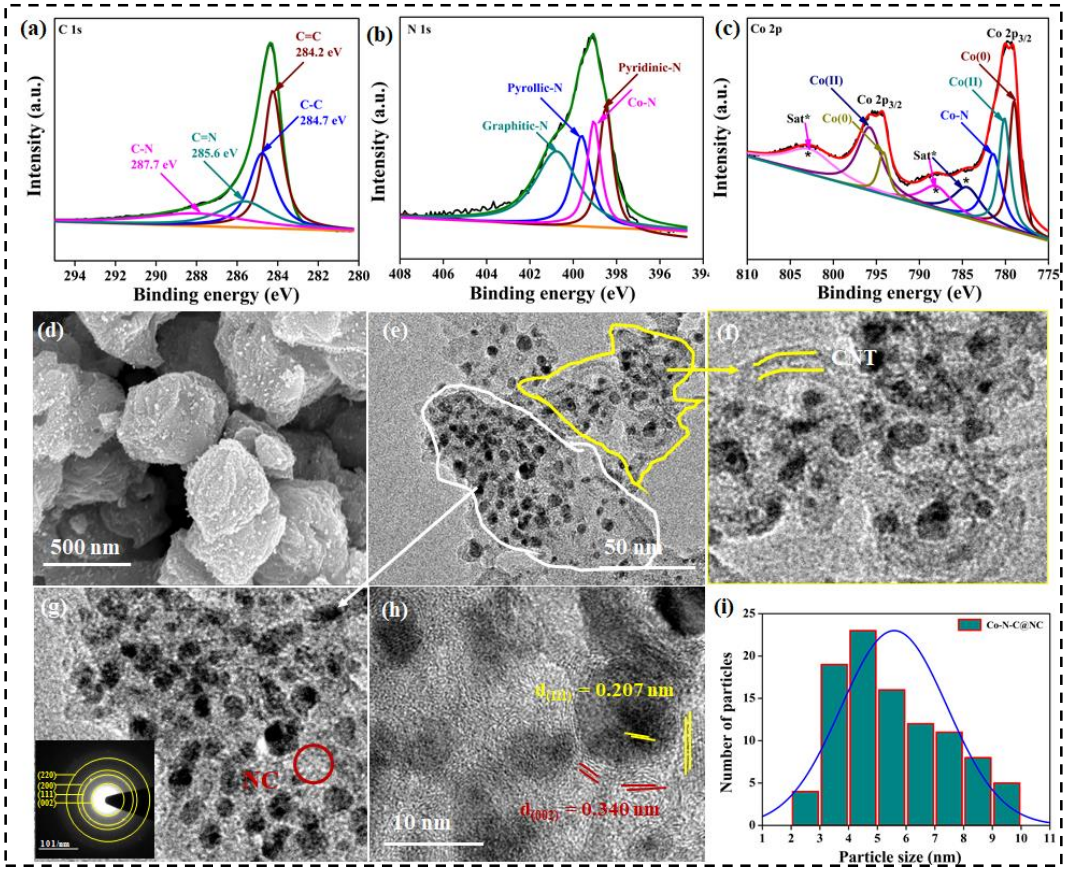

Figure 3.2: (a) The C 1s spectrum of Co−N−C@NC was deconvoluted into four peaks for C=C, C−C, C=N, and C−N species. (b) The N 1s spectrum was fitted into four peaks- corresponding to pyridinic, Co−N, pyrrolic, and graphitic nitrogen. (c) Co 2p XPS was fitted into peaks for Co(0), Co−N, and Co(II) species. The * marked peaks originated as the satellite peaks of Co(II). (d) The SEM image of the Co−N−C@NC shows the dodecahedron-type morphology. (e) The TEM images of the Co−N−C@NC catalyst shows the nanoparticle nature with a different type of support such as CNT and NC in the image (f) and (g). (h) HR-TEM image of the Co−N−C@NC with d-spacing 0.207 and 0.340 nm of the cubic plane (111) and graphene (002). (i) The image shows the nanoparticle size between 2-10 nm.

3.6. Optimization of reaction conditions

The benzimidazole reaction of amines with alcohols was carried out in a 15 mL pressure-sealed tube. In a typical experiment, the sealed tube was filled with 1 mmol benzyl alcohol, 0.5 mmol *o*-phenylenediamine, 10 mg catalyst (Co−N−C@NC) and toluene (2 mL) was used as a solvent. Then, the nitrogen gas was purged in the tube, then tube was capped and placed in the oil bath preheated at 140 °C and the reaction was continued for 12 h with stirring (500 rpm) and monitored by TLC. After the reaction, the sealed tube was cooled down to room temperature and the mixture was centrifuged to separate the solid catalyst. The liquid part was collected and worked up. The % of conversion and product yield was analyzed using ^{1}H NMR.

The ZIF-67 derived Co−N−C@NC catalyst was used to optimized for the benzimidazole reaction from the *o*-phenylenediamine with benzyl alcohol (**Table 3.1**). The reaction of *o*-phenylenediamine and benzyl alcohol to produce 2-phenyl-1*H*-benzo[*d*]imidazole (**3a**) as the major products. The production of **3a** derived product was very useful in the industrial applications. The catalytic performance of Co−N−C@NC catalyst was produced high yield of benzimidazole products. Interestingly, the Co−N−C@NC was found very effective for the benzimidazole reactions. In the Co−N−C@NC catalyst the Co with N coordination improved the catalytic activity for the reactions. Therefore, the Co−N−C@NC catalyst was produced high yield 90% of **3a** product (**Entry 1, Table 3.1**).

The pyrolysis temperature was also affected the product yield. From the comparison purposes the pyrolysis temperature (700-900 ^{o}C), it was found that Co−N−C@NC (prepared at 800 ^{o}C) produced the best activity and selectivity for **3a** (**Entries 1-3, Table 3.1**). The Co@C catalyst was produced 54% selective product **3a** and when the benzimidazole reaction was carried out without catalyst to produced poor yield (**Entries 4-6, Table 3.1**). In the

Co−N−C@NC catalyst the Co with N coordination was found important role for the catalytic activity of the benzimidazole reaction.

Table 3.1 Optimization of the reaction condition

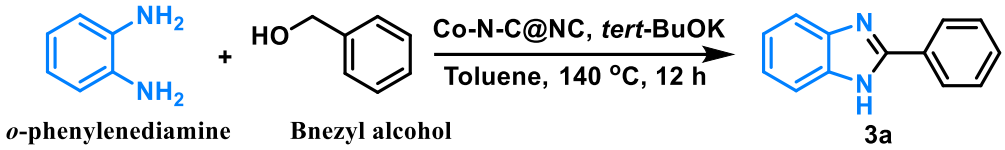

o-phenylenediamine Bnezyl alcohol 3a

Entry	Catalyst	Base	Solvent	Temp. (°C)	Conv. (%)	Yield **3a** (%)
Variation of catalysts						
1.	**Co-N-C@NC**	***tert*-BuOK**	**Toluene**	**140**	**100**	**90**
2.	Co-N-C@NC -1	*tert*-BuOK	Toluene	140	93	82
3.	Co-N-C@NC -2	*tert*-BuOK	Toluene	140	100	86
4.	Co@C	*tert*-BuOK	Toluene	140	65	54
5.	ZIF-67	*tert*-BuOK	Toluene	140	32	15
6.	-	*tert*-BuOK	Toluene	140	25	13
Variation of base						
7.	Co-N-C@NC	-	Toluene	140	60	45
8.	Co-N-C@NC	K_2CO_3	Toluene	140	66	52
9.	Co-N-C@NC	Cs_2CO_3	Toluene	140	80	66
10.	Co-N-C@NC	KOH	Toluene	140	88	71
11.	**Co-N-C@NC**	***tert*-BuOK**	**Toluene**	**140**	**100**	**90**
12.	Co-N-C@NC	*tert*-BuOK(0.1 mmol)	Toluene	140	64	50
13.	Co-N-C@NC	*tert*-BuOK(0.3 mmol)	Toluene	140	86	75
14.	**Co-N-C@NC**	***tert*-BuOK(0.5 mmol)**	**Toluene**	**140**	**100**	**90**
Variation of solvent						
15.	Co-N-C@NC	*tert*-BuOK	CH_3CN	140	63	48
16.	Co-N-C@NC	*tert*-BuOK	Dioxane	140	75	61
17.	Co-N-C@NC	*tert*-BuOK	THF	140	86	72
18.	**Co-N-C@NC**	***tert*-BuOK**	**Toluene**	**140**	**100**	**90**
Variation of Temperature						
19.	Co-N-C@NC	*tert*-BuOK	Toluene	100	54	40
20.	Co-N-C@NC	*tert*-BuOK	Toluene	120	77	64
21.	**Co-N-C@NC**	***tert*-BuOK**	**Toluene**	**140**	**100**	**90**

Reaction conditions: 0.75 mmol benzyl alcohol, 0.5 mmol of *o*-phenylenediamine, 0.5 mmol of *tert*-BuOK, toluene (2 mL), 140 °C, for 12 h.

The reaction condition was also optimized with the various bases K_2CO_3, KOH, Cs_2CO_3, and *test*-BuOK, the *test*-BuOK to produced high yield of **3a** product. And the amount of base also improved the product yield (**Entries 7-14, Table 3.1**). Further, we have optimized with various solvents CH_3CN, dioxane, THF and toluene and we found that an excellent yield was obtained with toluene solvent (**Entries 15-18, Table 3.1**). The reaction temperature was affected the **3a** product yield, it was optimized at 140 ^oC temperature produced high yield (**Entries 19-21, Table 3.1**).

3.7. Scope of alcohols

As the N-containing heterocyclic benzimidazole compounds are an important component in anticancer, antibacterial, antitumor, anti-HIV, and anthelmintic-related drugs. Inspired by the importance of the benzimidazole reactions and catalytic performance of the Co−N−C@NC catalyst, we have performed the substrate scope for the synthesis of various substituted benzimidazole products was investigated. By using this catalyst, the hydrogen transfer-dehydrogenative cyclization of benzyl alcohol with *o*-phenylenediamine derivatives was developed for the preparation of benzimidazole derivative products.

With the optimized reaction condition, we have studied different substituted benzimidazole reactions with the benzyl alcohol and *o*-phenylenediamine to obtain the yields 90-75% (**Scheme 3.3, 3a-3j and Table 3.1**). The strong electron-donating group of the substrates provides high yield of the product and electron crowding decrease yield of products (**Scheme 3.3, 3b-3e and Table 3.1)**. The electron-withdrawing group and alkyl substituted group decreases the yield of the product (**Scheme 3.3, 3f-3j and Table 3.1**).

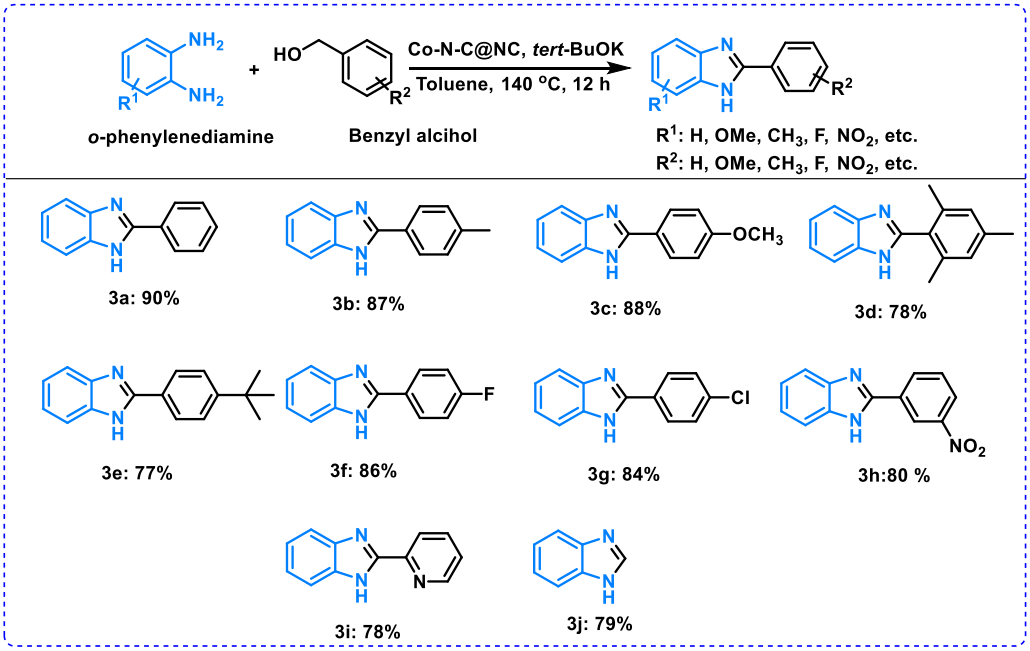

Scheme 3.2: The cyclization of benzimidazole reaction with Co−N−C@NC catalyst. Reaction conditions: 1 mmol benzyl alcohol, 0.5 mmol of *o*-phenylenediamine, 0.5 mmol of *tert*-BuOK, toluene (2 mL), 140 °C, for 12 h.

3.8. Reaction mechanism and recyclability

Thus, a plausible mechanism for the cyclization of benzyl alcohol and *o*-phenylenediamine to form 2-benzylbenzimidazole is proposed. First of all, benzyl-alcohol is adsorbed on the Co−N−C@NC catalyst and oxidized to benzaldehyde, at the same time, cobalt species with small particle sizes are easily activated to generate [Co]−H intermediate. Subsequently, on the surface of the Co−N−C@NC catalyst *o*-phenylenediamine couples with benzaldehyde via a condensation reaction to form imine intermediate. The imine intermediate undergoes intramolecular oxidative cyclization reaction under the action of Co−N−C@NC catalyst to form a cyclic intermediate, and then further it was dehydrogenated to form the corresponding product 3a. Moreover, the dispersed Co nanoparticles on the surface of the NC and N−doped CNTs support can expedite the dissociation of [Co]−H intermediate into the active hydrogen

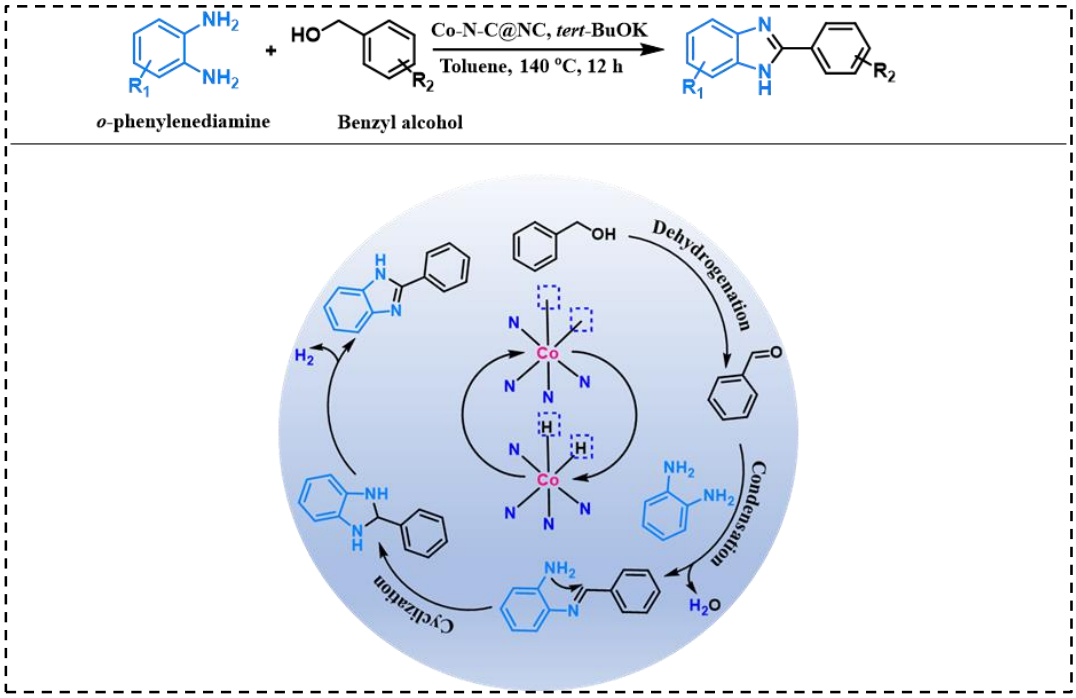

Scheme 3.3: Reaction mechanism of benzimidazole reaction with Co−N−C@NC catalyst.

(−[H]) on the surface of Co−N−C@NC catalyst, and rapidly re-oxidation dehydrogenation to form a cycle for the cyclization reaction and is called benzimidazole product.[47],[48a-b]

Recyclability is considered a crucial standard to assess catalysts in heterogeneous catalytic reactions. Hence, the recoverability of the Co−N−C@NC catalyst for cyclization reaction between *o*-phenylenediamine and benzyl-alcohol was conducted. After each cyclization reaction of the benzimidazole test, the catalyst was washed with acetone and ethanol separated by centrifugation several times, and dried overnight for further testing of the recyclability of the catalyst. The catalyst exhibits no significant loss throughout the six cycles. After, the recyclability of the catalyst, the catalyst was leached out 0.47% during the reaction.

3.9. Conclusions

In summary, the Co−N−C@NC catalyst was synthesized as a novel effective catalytic system for a wide variety of benzimidazole syntheses by hydrogen transfer-dehydrogenative

cyclization coupling of *o*-phenylenediamine substrates with benzyl alcohol. And achieved high yield (90%) of benzimidazole product and it was used as a biologically active compound for different diseases. In addition, the NC and N-doped CNT improved the charge transfer and electron density through the Co-N coordination and provided high catalytic active center for the benzimidazole reactions. The Co−N−C@NC catalysts are robust and recyclable more than five times with low loss of activity and selectivity for the benzimidazole reactions.

Table 3.2. Characterization of the products by ^{1}H NMR and ^{13}C NMR

3a: 2-phenyl-1*H*-benzo[*d*]imidazole 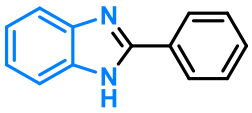	**^{1}H NMR (500 MHz, DMSO-D$_6$)** δ 12.95 (brs, 1H), 8.21 (d, J = 7.1 Hz, 2H), 7.73 – 7.47 (m, 5H), 7.22 (d, 2H). **^{13}C NMR (125 MHz, DMSO-D$_6$)** δ 151.72, 144.27, 135.44, 130.67, 130.30, 129.41, 126.92, 122.72, 122.20, 119.29, 111.82. Yield of product: 90%.
3b: 2-(*p*-tolyl)-1*H*-benzo[*d*]imidazole 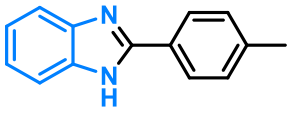	**^{1}H NMR (500 MHz, DMSO-D$_6$)** δ 12.71 (s, 1H), 8.05 (d, 2H), 7.62 (d, 1H), 7.56–7.43 (m, 1H), 7.31 (d, 2H), 7.23 – 7.07 (m, 2H), 2.32 (s, 3H); **^{13}C NMR (125 MHz, DMSO-D$_6$)** δ 151.94, 140.10, 130.06, 127.99, 126.93, 122.88, 111.75, 21.50. Yield of product: 87%.
3c: 2-(4-methoxyphenyl)-1*H*-benzo[*d*]imidazole 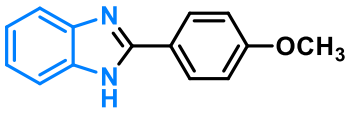	**^{1}H NMR (500 MHz, DMSO-D$_6$)** δ 12.78 (brs, 1H), 8.17 (d, J = 8.1 Hz, 2H), 7.60 (d, 2H), 7.21 (m, 2H), 7.15 (d, 2H), 3.88 (s, 3H). **^{13}C NMR (125 MHz, DMSO-D$_6$)** δ 160.71, 151.25, 128.09, 122.40, 121.91, 114.40, 55.36. Yield of product: 88%.
3d: 2-mesityl-1*H*-benzo[*d*]imidazole 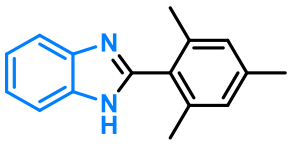	**^{1}H NMR (500 MHz, DMSO-D$_6$)** δ 12.73 (s, 1H), 7.93-7.73 (d, 2H), 7.53 (s, 1H), 7.45 (d, 2H), 7.23-7.15 (m, 2H), 2.45-2.41 (s, 6H), 2.38-2.34 (s, 3H). **^{13}C NMR (125 MHz, DMSO-D$_6$)** δ 152.18, 145.69, 141.50, 138.10, 137.13, 135.13, 133.70, 132.85, 130.85, 128.62, 126.33, 123.49, 119.12, 21.81, 20.73, 20.73. Yield of product: 78%.

3e: 2-(4-(*tert*-butyl)phenyl)-1*H*-benzo[*d*]imidazole 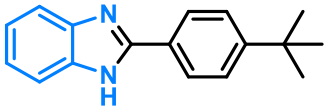	**^{1}H NMR (500 MHz, DMSO-D$_6$)** δ 12.74 (s, 1H), 8.12 (d, 2H), 7.63 – 7.56 (m, 4H), 7.21 (dd, 2H), 1.34 (s, 9H). **^{13}C NMR (125 MHz, DMSO-D$_6$)** δ 152.55,151.27, 143.84, 134.95, 127.44, 126.22, 125.72, 122.31, 121.53, 118.72, 111.19, 34.58, 30.98. Yield of product: 77%.
3f: 2-(4-fluorophenyl)-1*H*-benzo[*d*]imidazole 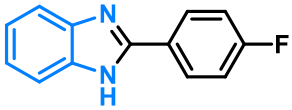	**^{1}H NMR (500 MHz, DMSO-D$_6$)** δ 12.75 (brs, 1H), 8.13 (d, J = 8.7 Hz, 2H), 7.56 – 7.53 (m, 2H), 7.25 (d, 2H), 7.20 (d, 2H). **^{13}C NMR (125 MHz, DMSO-D$_6$)** δ 163.11, 161.49, 160.06, 151.74, 133.48, 130.59, 130.53 128.48, 123.44, 115.84, 115.67. Yield of product: 86%,
3g: 2-(4-chlorophenyl)-1*H*-benzo[*d*]imidazole 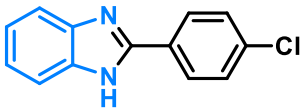	**^{1}H NMR (500 MHz, DMSO-D$_6$)** δ 12.85 (s, 1H), 8.15 (d, J = 8.5 Hz, 2H), 7.66 –7.55 (m, 4H), 7.25–7.20 (m, 2H). **^{13}C NMR (125 MHz, DMSO-D$_6$)** δ 163.11, 161.49, 160.06, 151.74, 133.48, 130.59, 130.53 128.48, 123.44, 115.84, 115.67. Yield of product: 84%,
3h: 2-(3-nitrophenyl)-1*H*-benzo[*d*]imidazole 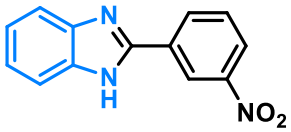	**^{1}H NMR (500 MHz, DMSO- D6)** δ 12.95 (s, 1H), 9.03 (s, 1H), 8.61 (d, 1H), 8.37 (d, 1H), 7.89 (t, 1H), 7.70 (dd, , 2H), 7.33 (dd, J = 6.0, 3.1, 2H). Yield of product: 80%,
3i: 2-(pyridine-2-yl)-1*H*-benzo[*d*]imidazole 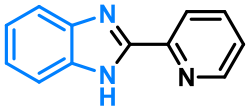	**^{1}H NMR (500 MHz, DMSO-D$_6$)** δ 13.02 (s, 1H), 8.65 (d, 1H), 8.30 (d, 1H), 8.05 (td, 1H), 7.70 (d, 1H), 7.54-7.45 (m, 2H), 7.25-7.20 (m, 2H). Yield of product: 78%,
3j: 1*H*-benzo[*d*]imidazole 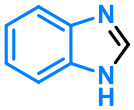	**^{1}H NMR (500 MHz, DMSO-D$_6$)** δ 8.9 (s, 1H), 7.98-7.74 (m, 2H), 7.52 (d, 2H), 7.23 (s, 1H). **^{13}C NMR (125 MHz, DMSO-D$_6$)** δ 162.34, 152.25, 147.02, 132.45, 129.71, 123.85, 120.01. Yield of product: 79%.

3.10. ^{1}H NMR and ^{13}C NMR spectra of product

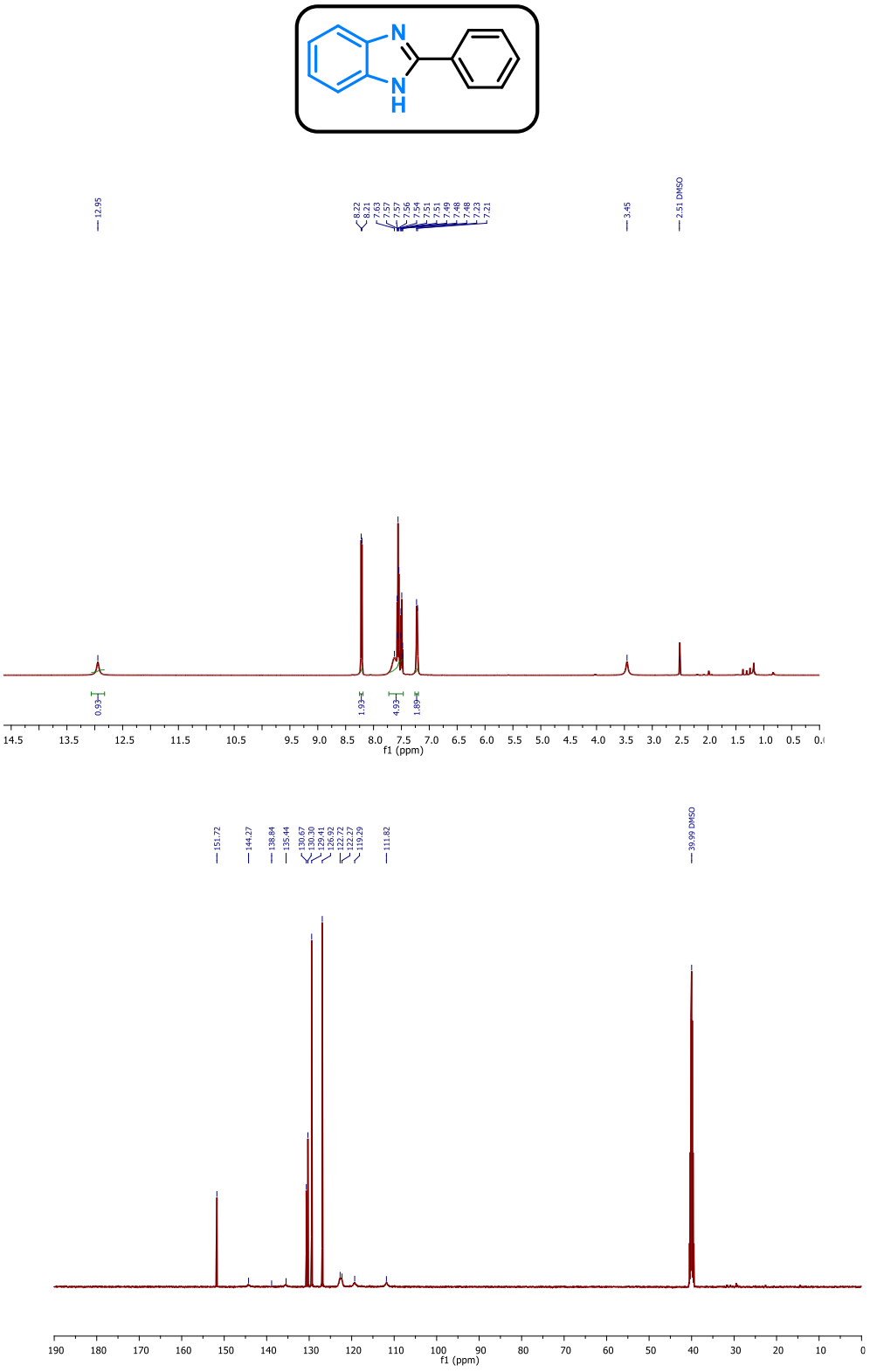

Figure 3.3. ^{1}H NMR and ^{13}C NMR spectra of the product **3a.**

3.11. Reference:

[1] A. Bera, M. Sk, K. Singh, D. Banerjee, *Chem. Commun.* **2019**, *55*, 5958–5961.

[2] M. Maji, D. Panja, I. Borthakur, S. Kundu, *Org. Chem. Front.* **2021**, *8*, 2673–2709.

[3] Z. Sun, G. Bottari, K. Barta, *Green Chem.* **2015**, *17*, 5172–5181.

[4] V. A. Mamedov, *RSC Adv.* **2016**, *6*, 42132–42172.

[5] S. Kumari, A. Joshi, I. Borthakur, S. Kundu, *J. Org. Chem.* **2023**, *88*, 11523–11533.

[6] X. Hui, J. Desrivot, C. Bories, P. M. Loiseau, X. Franck, R. Hocquemiller, B. Figadère, *Bioorganic Med. Chem. Lett.* **2006**, *16*, 815–820.

[7] B. Pathare, T. Bansode, *Results Chem.* **2021**, *3*, 100200.

[8] C. S. W. Law, K. Y. Yeong, *ChemMedChem* **2021**, *16*, 1861–1877.

[9] D. Diaconu, V. Antoci, V. Mangalagiu, D. Amariucai-Mantu, I. I. Mangalagiu, *Sci. Rep.* **2022**, *12*, 1–17.

[10] Y. B. Kim, Y. H. Kim, J. Y. Park, S. K. Kim, *Bioorganic Med. Chem. Lett.* **2004**, *14*, 541–544.

[11] R. Zamudio-Vázquez, S. Ivanova, M. Moreno, M. I. Hernandez-Alvarez, E. Giralt, A. Bidon-Chanal, A. Zorzano, F. Albericio, J. Tulla-Puche, *Chem. Sci.* **2015**, *6*, 4537–4549.

[12] Y. Qin, M. Hao, C. Xu, Z. Li, *Green Chem.* **2021**, *23*, 4161–4169.

[13] T. Irrgang, R. Kempe, *Chem. Rev.* **2019**, *119*, 2524–2549.

[14] P. Anandaraj, R. Ramesha, J. G. Malecki, *J. Organomet. Chem.* **2023**, *985*, 122577.

[15] Z. Dehbanipour, A. Zarnegareyan, *Inorg. Chem. Commun.* **2022**, *141*, 109513.

[16] Z. Z. Nori, A. Landarani-Isfahani, M. Bahadori, M. Moghadam, V. Mirkhani, S. Tangestaninejad, I. Mohammadpoor-Baltork, *RSC Adv.* **2020**, *10*, 33137–33147.

[17] S. Gayathri, P. Viswanathamurthi, R. Bertani, P. Sgarbossa, *ACS Omega* **2022**, *7*, 33107–33122.

[18] W. H. Tang, Y. H. Liu, S. M. Peng, S. T. Liu, *J. Organomet. Chem.* **2015**, *775*, 94–100.

[19] K. Chakrabarti, M. Maji, S. Kundu, *Green Chem.* **2019**, *21*, 1999–2004.

[20] T. Hille, T. Irrgang, R. Kempe, *Chem. A Eur. J.* **2014**, *20*, 5569–5572.

[21] J. Zhang, R. Yao, J. Chen, T. Li, Y. Xu, *Science* **2021**, *24*, 103045.

[22] Z. Nawaz, H. Ullah, N. Gürbüz, M. N. Zafar, F. Verpoort, M. N. Tahir, I. Özdemir, R. J. Trovitch, *Mol. Catal.* **2022**, *526*, 112369.

[23] L. Chen, Y. Zhang, Y. Zhou, G. hui Li, X. song Feng, *J. Chromatogr. A* **2021**, *1644*, 462068.

[24] K. Das, A. Mondal, D. Srimani, *Chem. Commun.* **2018**, *54*, 10582–10585.

[25] B. Guo, H. X. Li, S. Q. Zhang, D. J. Young, J. P. Lang, *ChemCatChem* **2018**, *10*, 5627–5636.

[26] P. Daw, A. Kumar, N. A. Espinosa-Jalapa, Y. Diskin-Posner, Y. Ben-David, D.

Milstein, *ACS Catal.* **2018**, *8*, 7734–7741.
[27] S. Shee, K. Ganguli, K. Jana, S. Kundu, *Chem. Commun.* **2018**, *54*, 6883–6886.
[28] A. K. Bains, V. Singh, D. Adhikari, *J. Org. Chem.* **2020**, *85*, 14971–14979.
[29] H. Li, Y. Zhang, Z. Yan, Z. Lai, R. Yang, M. Peng, Y. Sun, J. An, *Green Chem.* **2022**, *24*, 748–753.
[30] L. Hao, Y. Zhao, B. Yu, H. Zhang, H. Xu, Z. Liu, *Green Chem.* **2014**, *16*, 3039–3044.
[31] A. K. Bains, D. Dey, S. Yadav, A. Kundu, D. Adhikari, *Catal. Sci. Technol.* **2020**, *10*, 6495–6500.
[32] T. Song, P. Ren, Z. Ma, J. Xiao, Y. Yang, *ACS Sustain. Chem. Eng.* **2020**, *8*, 267–277.
[33] Y. Chen, X. Sun, Y. Sha, X. Fang, W. Chu, X. Wang, *Mol. Catal.* **2023**, *545*, 113186.
[34] P. Daw, Y. Ben-David, D. Milstein, *ACS Catal.* **2017**, *7*, 7456–7460.
[35] T. Chen, W. Yu, C. K. T. Wun, T. S. Wu, M. Sun, S. J. Day, Z. Li, B. Yuan, Y. Wang, M. Li, Z. Wang, Y. K. Peng, W. Y. Yu, K. Y. Wong, B. Huang, T. Liang, T. W. B. Lo, *J. Am. Chem. Soc.* **2023**, 3c00114.
[36] Y. F. Wang, M. Y. Qi, M. Conte, Z. R. Tang, Y. J. Xu, *Angew. Chem. Int. Ed.* **2023**, *62*, 04306.
[37] G. Zhu, Z. C. Duan, H. Zhu, D. Ye, D. Wang, *Chinese Chem. Lett.* **2022**, *33*, 266–270.
[38] S. Verma, S. Kujur, R. Sharma, D. D. Pathak, *ACS Omega* **2022**, *7*, 9754–9764.
[39] M. J. Climent, A. Corma, J. C. Hernández, A. B. Hungría, S. Iborra, S. Martínez-Silvestre, *J. Catal.* **2012**, *292*, 118–129.
[40] S. Aryanejad, G. Bagherzade, A. Farrokhi, *Inorg. Chem. Commun.* **2017**, *81*, 37–42.
[41] A. Ramalingam, G. C. Senadi, *Asian J. Org. Chem.* **2023**, *12*, 00119.
[42] Y. Xiong, K. Wang, L. Ma, J. Zhu, Y. Miao, L. Gong, X. Mu, J. Wan, R. Li, *Appl. Organomet. Chem.* **2022**, *36*, 1–12.
[43] S. Ma, W. Han, W. Han, F. Dong, Z. Tang, *J. Mater. Chem. A* **2023**, *11*, 3315–3363.
[44] Y. L. Lai, J. S. Ye, J. M. Huang, *Chem. A Eur. J.* **2016**, *22*, 5425–5429.
[45] V. Sankar, P. Karthik, B. Neppolian, B. Sivakumar, *New J. Chem.* **2020**, *44*, 1021–1027.
[46] C. Li, L. L. Zhang, H. Li, S. Yang, *Front. Chem. Sci. Eng.* **2023**, *17*, 68–81.
[47] K. Sun, D. Li, G. P. Lu, C. Cai, *ChemCatChem* **2021**, *13*, 373–381.
[48] (a) C. Lin, W. Wan, X. Wei, J. Chen, *ChemSusChem* **2021**, *14*, 709–720. (b) S. Das, S. Mallick, S. D. Sarkar, *J. Org. Chem.* **2019**, *18*, 12111–12119.
[49] B. Wang, M. Li, S. Zhang, H. Wu, Y. Liao, H. Li, *Appl. Catal. B Environ.* **2023**, *327*, 122454.
[50] Z. Ye, J. Chen, *ACS Catal.* **2021**, *11*, 13983–13999.
[51] X. Zhao, B. Pattengale, D. Fan, Z. Zou, Y. Zhao, J. Du, J. Huang, C. Xu, *ACS Energy Lett.* **2018**, *3*, 2520–2526.
[52] C. Li, Y. Meng, S. Yang, H. Li, *ChemCatChem* **2021**, *13*, 5166–5177.

[53] T. Y. Su, G. P. Lu, K. K. Sun, M. Zhang, C. Cai, *Catal. Sci. Technol.* **2022**, *12*, 2106–2121.

[54] A. Baghban, H. Ezedin Nejadian, S. Habibzadeh, F. Zokaee Ashtiani, *Sci. Rep.* **2022**, *12*, 1–13.

[55] R. Wang, K. Lu, J. Zhang, X. Li, Z. Zheng, *ACS Catal.* **2022**, *12*, 14290–14303.

[56] A. K. Singh, S. Ji, B. Singh, C. Das, H. Choi, P. W. Menezes, A. Indra, *Mater. Today Chem.* **2022**, *23*, 100668.

[57] J. Lu, Y. Zeng, X. Ma, H. Wang, L. Gao, H. Zhong, Q. Meng, *Polymers.* **2019**, *11*, 11050828.

[58] Y. Li, F. Cheng, J. Zhang, Z. Chen, Q. Xu, S. Guo, *Small* **2016**, *12*, 2839–2845.

[59] Y. Jiang, K. Dong, X. Yan, C. Chen, P. Ni, C. Yang, Y. Lu, *Sustain. Energy Fuels* **2020**, *4*, 3370–3377.